Relativistic distorted-wave Born calculations for $(e,2e)$ processes on inner shells of heavy atoms

S. Keller,* Colm T. Whelan, and H. Ast
Department of Applied Mathematics and Theoretical Physics, University of Cambridge, Silver Street, Cambridge CB3 9EW, United Kingdom

H. R. J. Walters
Department of Applied Mathematics and Theoretical Physics, The Queen's University of Belfast, Belfast BT7 1NN, United Kingdom

R. M. Dreizler
Institut für Theoretische Physik der Universität, Robert-Mayer-Straße 6-8, 60054 Frankfurt/Main, Federal Republic of Germany
(Received 6 June 1994)

The theory and numerical methods required for extending the distorted-wave Born approximation to the description of relativistic $(e,2e)$ processes are developed. We compare the results of our theoretical approach with the absolute experimental data available in coplanar asymmetric geometry. A significant improvement over earlier calculations is achieved. It is shown that both the shape and the absolute magnitude of the triple differential cross section are strongly influenced by elastic electron-nucleus collisions in the incident and final channels. We predict an important increase of the magnitude relative to the binary peak and changes in shape of the secondary maximum of the triple differential cross section as a function of the nuclear charge.

PACS number(s): 34.80.Dp, 12.20.Ds

I. INTRODUCTION

The measurement of triple differential cross sections (TDCS) in electron-impact ionization experiments on atomic targets, pioneered by Ehrhardt *et al.* [1] and Amaldi *et al.* [2] has developed into one of the most sophisticated methods for studying the details of both the target structure and the scattering process itself. In these $(e,2e)$ experiments, the cross sections are determined as functions of the energies and emission angles of both outgoing electrons, so that the scattering kinematics are completely known. This provides a serious challenge to any theoretical description of the process. Indeed, to date no theory is capable of explaining all experimental results. Still, important insights have been gained by comparison of the data with different theoretical models. The current status of this field of research is reviewed in [3].

While most of the experiments and calculations have been devoted to nonrelativistic $(e,2e)$ processes, Nakel and collaborators have performed a number of absolute measurements of K-shell ionization TDCS for heavy atoms [4–8]. Due to the large binding energies involved, relativistic electrons are required for the ionization process. All theoretical studies of these relativistic $(e,2e)$ experiments reported so far have used modifications of the first-order Born approximation. The most straightforward calculation was that of Bell [9] who used plane waves to represent all unbound electrons and the impulse approximation to factorize the TDCS into the momentum profile of the bound state and the free electron-electron scattering cross section. In earlier work, Das and Konar [10] had employed a semirelativistic Sommerfeld-Maue function for one of the outgoing electrons. Subsequently, in a series of calculations, Jakubaβa-Amundsen studied the influence of the choice of different approximate semirelativistic scattering and bound-state wave functions on the TDCS [11,12]. Walters *et al.* [7] demonstrated the need to incorporate purely relativistic spin-flip processes in calculations of the TDCS in symmetric geometry. All these calculations overestimate the experimental cross sections. This overestimation is most pronounced for the heaviest target considered (Au).

It is argued in [7] that the distorting effect of both the strong nuclear potential and the electrostatic potential of the electron cloud must be taken into account for inner-shell ionization in all geometries. This observation is supported by the excellent agreement of calculations in the distorted-wave Born approximation (DWBA) [13,14] with experimental results for the inner-shell ionization of neon and argon at nonrelativistic impact energies. This approximation allows for elastic scattering of the incident and outgoing electrons in the field of the atom or ion

*Present address: Institut für Theoretische Physik der Universität, Robert-Mayer-Straβe 6-8, 60054 Frankfurt/Main, Federal Republic of Germany.

while the ionization is described in terms of a first-order electron-electron interaction. To achieve this, the wave functions describing the unbound electrons have to be constructed numerically as scattering eigenstates of the Schrödinger equation using appropriate effective potentials.

The numerical solution of the wave equation can be avoided if the distorted waves are approximated by nonrelativistic Coulomb waves that are known analytically. A careful analysis of this "Coulomb-Born" approximation has been carried out by Botero and Macek [15] for the K-shell ionization of carbon by fast, but nonrelativistic, electrons. They explicitly demonstrate the crucial importance of properly including the phases of the various contributions to the S matrix that may be expected to be strongly influenced by the electron-nucleus elastic-scattering phase shifts for heavier atoms. Indeed the Coulomb-Born calculations of Refs. [11,12] have up to now provided the most adequate description of relativistic $(e,2e)$ processes, though they also seriously overpredict the experimental TDCS for the experiments with gold targets.

While taking into account the influence of the nuclear potential, apart from the inconsistency of using nonrelativistic wave functions to describe a relativistic process, the Coulomb-Born approximation has the obvious defect of completely neglecting the electrostatic potential generated by the spectator target electrons in its description of the unbound particles. Now it is known that even at relativistic impact energies the elastic differential scattering cross section differs considerably from the Coulomb scattering result [16]. Furthermore, for a quantitative understanding of experimental bremsstrahlung differential cross sections at these energies, the use of an effective atomic potential rather than a Coulomb potential is essential [17]. These results provide strong evidence for a major influence of the effective atomic field on the TDCS of relativistic $(e,2e)$ processes. Therefore a fully relativistic extension of the distorted-wave Born approximation suggests itself as an appropriate theoretical framework for the study of these processes.

In the present paper we develop the theory of relativistic $(e,2e)$ processes using exact eigenstates of the Dirac equation with an effective atomic potential for all electron wave functions. That is, we calculate the two-particle S-matrix elements of quantum electrodynamics (QED) to lowest order in the electron-electron interaction coupling constant α, but to all orders in the effective electron-nucleon interaction coupling $Z(r)\alpha$ (where $Z\alpha$ is of order unity for the heavy targets used in the experiments mentioned above and the notation indicates the inclusion of screening by the atomic electrons). On the other hand, the method employed may be viewed as the direct generalization of the distorted-wave Born approximation discussed above, employing (partial-wave expanded) Dirac spinors instead of Schrödinger wave functions and the full QED photon propagator (in a generalized multipole expansion) as the relativistic generalization of the interelectronic Coulomb potential.

Relativistic distorted-wave Born calculation of single differential electron-impact ionization cross sections have been the subject of a series of papers by Pindzola and collaborators [18–22]. The formalism developed in [19] is essentially equivalent to the one employed in the present contribution. However, the calculation of angle differential cross sections, which is the objective of our work, turns out to be a much more formidable task. This has been noted by Butler *et al.* [23] who studied positron-impact ionization cross sections using the same method. While these authors could calculate cross sections as a function of the impact energy using only a few multipoles and partial waves, they found it impossible to obtain satisfactory convergence of the multiple sums for TDCS. Up to now, apart from results of a first set of our own calculations [24], within the relativistic distorted-wave Born approximation angle differential cross sections have only been obtained for bremsstrahlung [17] and electron positron pair creation induced by internal nuclear conversion [25], that is, for one-fermion matrix elements.

At this point, it is also worth noticing that a very similar method has a long tradition in the study of QED effects in heavy atomic systems. Indeed, the formalism we derive in the following section is closely related to the Wichmann-Kroll [26] approach to the calculation of QED corrections in strong Coulomb fields. The latter approach is the basis of some of the most refined calculations of vacuum polarization [27], electron self-energies [28], and Delbrück scattering [29]. In these calculations an additional complication arises from the necessity of performing a sum over energy eigenstates to construct the off-shell fermion propagator in the external field. Also, the renormalization problem has to be faced. On the other hand, in computing QED effects it is usual practice to disregard the influence of the potential generated by the remaining electrons, i.e., to work with a pure Coulomb potential plus an analytical model for the potential inside the nucleus. This fact can be exploited to simplify the numerical calculations considerably.

The present paper is organized as follows. In Sec. II we develop the formal theory underlying our calculations. The methods used for the numerical evaluation of the resulting expressions are presented in Sec. III. We discuss in some detail the question of convergence of the multipole and partial-wave expansions. In Sec. IV, we present numerical data for triple differential cross sections in coplanar asymmetric geometry corresponding to measurements by Nakel and collaborators. (A preliminary account of some of these results has been given in [24].) Section V consists of a summary of our results and an outlook of future refinements and extensions to our work.

In the following, atomic units ($\hbar = m_e = e = 1$) are used so that the numerical value of the vacuum velocity of light is $c = 137.036\,04$. The metric tensor has $\mathrm{diag}\, g_{\mu\nu} = (1,-1,-1,-1)$; contravariant four vectors are written as $x^\mu = (t,\mathbf{x})$. The summation convention is understood.

II. THEORY

The TDCS for a relativistic $(e,2e)$ process at a given impact energy E_0 is defined by

$$\frac{d^3\sigma_{(e,2e)}}{d\Omega_1 d\Omega_2 dE_2}=\frac{(2\pi)^2}{c^6}\frac{k_1k_2}{k_0}E_0E_1E_2\frac{N_\kappa}{2N_m}\sum_{\epsilon_1\epsilon_0\epsilon_2\epsilon_b}|\langle k_1\epsilon_1,k_2\epsilon_2|\hat{S}|k_0\epsilon_0,\kappa\epsilon_b\rangle|^2\ , \tag{1}$$

where $\hat{S}$ is the S matrix operator. Throughout this paper the indices 0, 1, 2, and b refer to the incoming, the two outgoing, and the initially bound electron, respectively. E_0, E_1, E_2 and k_0, k_1, k_2 are the on-shell total energies and momenta of the unbound particles $E^2=k^2c^2+c^4$. The quantity κ denotes the quantum numbers of the atomic bound state (see below) and ϵ are the spin projections with respect to the quantization axis, which we define to be the beam axis. Since we presently deal only with experiments that are insensitive to spin polarization, Eq. (1) involves a sum over the final spin states ϵ_1,ϵ_2 and an average over the initial ones (ϵ_0 and ϵ_b); hence the factor of $N_\kappa/2N_m$ (N_κ is the occupation number of the state κ, N_m the number of degenerate states with this set of quantum numbers).

For any process involving relativistic electrons and electromagnetic fields, the S-matrix operator is formally defined within QED. Of course, a complete evaluation of this quantity is not feasible. Indeed, due to its enormous complexity, such a solution would not be very helpful in understanding the physical processes involved. We therefore introduce the following approximations.

(a) The electromagnetic fields of the nucleus and of the atomic electrons are incorporated in the form of a classical external field.

(b) The interaction of the two active electrons is treated in first-order perturbation theory, whereas the influence of the external field on all states is retained exactly.

These assumptions imply that all many-body effects (for instance, polarization of the atomic electron cloud or radiative corrections) may only enter the calculation via the external potential. The relativistic distorted-wave Born approximation thus defined corresponds to the evaluation of the two Feynman diagrams depicted in Fig. 1, or to a first-order calculation in the Furry picture of QED [30]. The physical process it describes may be visualized as a binary collision of the two electrons combined with elastic scattering of both the incoming and the two outgoing electrons off the atomic core.

By applying standard Feynman rules to interpret the diagrams in Fig. 1 (see, e.g., [31]) it is readily shown that the S-matrix element in question reads

$$\langle k_1\epsilon_1,k_2\epsilon_2|\hat{S}|k_0\epsilon_0,\kappa\epsilon_b\rangle^{\mathrm{DWBA}}=S^{\mathrm{dir}}-S^{\mathrm{ex}}\ , \tag{2a}$$

with

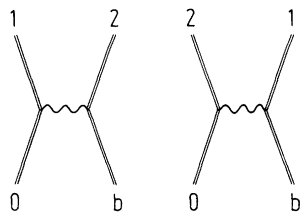

FIG. 1. Feynman diagrams corresponding to Eq. (2a).

$$S^{\mathrm{dir}}=i\int d^4x\int d^4y\,\psi^\dagger_{k_1,\epsilon_1}(x)\gamma^0\gamma^\mu\psi_{k_0,\epsilon_0}(x)\times D_{\mu\nu}(x-y)\psi^\dagger_{k_2,\epsilon_2}(y)\gamma^0\gamma^\nu\psi_{\kappa,\epsilon_b}(y)\ , \tag{2b}$$

$$S^{\mathrm{ex}}=i\int d^4x\int d^4y\,\psi^\dagger_{k_2,\epsilon_2}(x)\gamma^0\gamma^\mu\psi_{k_0,\epsilon_0}(x)\times D_{\mu\nu}(x-y)\psi^\dagger_{k_1,\epsilon_1}(y)\gamma^0\gamma^\nu\psi_{\kappa,\epsilon_b}(y)\ , \tag{2c}$$

where $D_{\mu\nu}(x-y)$ is the QED photon propagator (in the Feynman gauge) defined by

$$D_{\mu\nu}(x-y)=-\frac{4\pi}{c}ig_{\mu\nu}\int\frac{d^4q}{(2\pi)^4}\frac{e^{-iq(x-y)}}{q^2+i\eta},\quad \eta\to 0\ . \tag{2d}$$

Note that in writing Eqs. (2) we have reverted to first quantized notation. In particular, $\psi_{k,\epsilon}(x)$ is an exact stationary solution of the first quantized Dirac equation

$$i\frac{\partial}{\partial t}\psi(x)=\{\boldsymbol{\alpha}[-ic\nabla_x-\mathbf{A}(x)]+\beta c^2+V(x)\}\psi(x)\ . \tag{3}$$

[$\boldsymbol{\alpha}$, β, and γ^σ are the usual Dirac matrices; ($V(x)$, $\mathbf{A}(x)$) is the electromagnetic four-potential.] In the following discussion we will write all formulas only for the direct term. The exchange term follows by interchanging all quantum numbers of the outgoing electrons.

In order to evaluate (2) with (3) we introduce our final approximation, namely, the assumption that the external electromagnetic field is in fact purely electrostatic and radial symmetric in the rest frame of the nucleus (which we now choose as our reference frame):

$$\mathbf{A}(x)=\mathbf{0}\ , \tag{4a}$$

$$V(x)=V(r_x)\ . \tag{4b}$$

Then, the Dirac equation (3) can be separated in spherical coordinates $\mathbf{x}=(r_x,\hat{\Omega}_x)$. Solutions of this equation have the form

$$\psi(x)=e^{iEt/c}\begin{bmatrix} g_\kappa(r_x)\Xi_{\kappa,\mu}(\hat{\Omega}_x)\\ if_\kappa(r_x)\Xi_{-\kappa,\mu}(\hat{\Omega}_x)\end{bmatrix}, \tag{5}$$

where the quantum number $\kappa=-(2j+1)(j-l)$ represents good total angular momentum j and parity $(-1)^l$. The corresponding eigenstates with total angular momentum projection μ are spinorial harmonics defined by

$$\Xi_{\kappa,\mu}(\hat{\Omega}_x)=\sum_{m=-1/2}^{1/2}C(l,\tfrac{1}{2},j,\mu-m,m,\mu)Y_{l,\mu-m}(\Omega_x)\chi_m\ . \tag{6}$$

Here $C(\ldots)$ is a vector coupling coefficient (for which we use the conventions of [32]), $Y_{l,m}$ is a spherical harmonic, and χ_m is a two-component Pauli spinor. The radial wave functions are solutions of the equations

$$\frac{dg_\kappa(r)}{dr}+\frac{1+\kappa}{r}g_\kappa(r)+\frac{1}{c}[V(r)-c^2-E]f_\kappa(r)=0\ , \tag{7a}$$

$$\frac{df_\kappa(r)}{dr}+\frac{1-\kappa}{r}f_\kappa(r)-\frac{1}{c}[V(r)+c^2-E]g_\kappa(r)=0\ . \tag{7b}$$

In order to construct scattering waves with asymptotic linear momentum $\mathbf{k}$, spin projection ϵ, and the proper incoming or outgoing wave behavior, Eqs. (7) have to be solved subject to the boundary conditions

$$g_\kappa(r)\to\left|\frac{E+c^2}{2E}\right|^{1/2}\frac{1}{kr}\cos(kr+\delta_\kappa)\ , \tag{8a}$$

$$f_\kappa(r)\to-\left|\frac{E+c^2}{2E}\right|^{1/2}\frac{kc}{E+c^2}\frac{1}{kr}\sin(kr+\delta_\kappa)\ , \tag{8b}$$

for $r\to\infty$ where δ_κ is the scattering phase shift (that may include a logarithmic Coulomb phase). The solutions desired are then given by

$$\psi^{(\pm)}_{\mathbf{k},\epsilon}(t,\mathbf{x})=\frac{e^{iEt/c}}{(2\pi)^{3/2}}\sum_{j=1/2}^{\infty}\sum_{l=j-1/2}^{j+1/2}\sum_{\mu=-j}^{j}a^{(\pm)}(j,l,\epsilon,\mu)\begin{pmatrix}g_\kappa(r_x)\Xi_{\kappa,\mu}(\hat\Omega_x)\\ if_\kappa(r_x)\Xi_{-\kappa,\mu}(\hat\Omega_x)\end{pmatrix}\ , \tag{9a}$$

$$a^{(\pm)}(j,l,\epsilon,\mu)=4\pi i^l e^{\pm i[\delta_\kappa+\pi/2(l+1)]}C(l,\tfrac{1}{2},j,\mu-\epsilon,\epsilon,\mu)Y^*_{l,\mu-\epsilon}(\hat\Omega_k)\ . \tag{9b}$$

See [33,34] for details.

The photon propagator ($2d$) can also be represented in polar coordinates by writing it as a Fourier integral, doing the energy integration and expanding the result in multipoles. This leads to the representation

$$D_{\mu\nu}(x-y)=-8\pi^3\rho g_{\mu\nu}\sum_{n=0}^{\infty}\sum_{m=-n}^{n}j_n(\rho r_<)[-y_n(\rho r_>)+ij_n(\rho r_>)]Y^*_{nm}(\Omega_x)Y_{nm}(\Omega_y)\ , \tag{10}$$

where j_n and y_n are spherical Bessel functions of the first and second kind, $\rho:=(E_0-E_1)/c$ is the zero component of momentum transfer, $r_>:=\max(r_x,r_y)$, and $r_<:=\min(r_x,r_y)$. It is straightforward to show that, in the nonrelativistic limit ($c\to\infty$), Eq. (10) reduces to the well-known multipole expansion of the Coulomb potential between two point charges located at $\mathbf{x}$ and $\mathbf{y}$.

To evaluate the DWBA S-matrix elements, (9) and (10) are inserted into (2). After doing the time integrals, resolving the bispinor structure by inserting the γ matrices in the standard (Dirac) representation, and writing out the sum over Lorentz indices, this yields (with $\bar l=2j-l$)

$$\begin{aligned}S^{\rm dir}=&\,8\pi^2 i\rho\,\delta(E_0+E_b-E_1-E_2)\\
&\times\sum_{n,m}\int d^3x\int d^3y\,j_n(\rho r_<)[-y_n(\rho r_>)+ij_n(\rho r_>)]Y^*_{nm}(\hat\Omega_x)Y_{nm}(\hat\Omega_y)\\
&\times\sum_{j_1,l_1,\mu_1}\sum_{j_0,l_0,\mu_0}\sum_{j_2,l_2,\mu_2}[a^{(-)}(j_1,l_1,\epsilon_1,\mu_1)]^*a^{(+)}(j_0,l_0,\epsilon_0,\mu_0)[a^{(-)}(j_2,l_2,\epsilon_2,\mu_2)]^*\\
&\times\{[g_{E_1,\kappa_1}(r_x)g_{E_0,\kappa_0}(r_x)\Xi^*_{j_1,l_1,\mu_1}(\hat\Omega_x)\Xi_{j_0,l_0,\mu_0}(\hat\Omega_x)\\
&\quad+f_{E_1,\kappa_1}(r_x)f_{E_0,\kappa_0}(r_x)\Xi^*_{j_1,\bar l_1,\mu_1}(\hat\Omega_x)\Xi_{j_0,\bar l_0,\mu_0}(\hat\Omega_x)]\\
&\quad\times[g_{E_2,\kappa_2}(r_y)g_{E_b,\kappa_b}(r_y)\Xi^*_{j_2,l_2,\mu_2}(\hat\Omega_y)\Xi_{j_b,l_b,\mu_b}(\hat\Omega_y)\\
&\qquad+f_{E_2,\kappa_2}(r_y)f_{E_b,\kappa_b}(r_y)\Xi^*_{j_2,\bar l_2,\mu_2}(\hat\Omega_y)\Xi_{j_b,\bar l_b,\mu_b}(\hat\Omega_y)]\\
&\qquad+\sum_{i=1}^{3}[g_{E_1,\kappa_1}(r_x)f_{E_0,\kappa_0}(r_x)\Xi^*_{j_1,l_1,\mu_1}(\hat\Omega_x)\sigma^i\Xi_{j_0,\bar l_0,\mu_0}(\hat\Omega_x)\\
&\qquad\quad-f_{E_1,\kappa_1}(r_x)g_{E_0,\kappa_0}(r_x)\Xi^*_{j_1,\bar l_1,\mu_1}(\hat\Omega_x)\sigma^i\Xi_{j_0,l_0,\mu_0}(\hat\Omega_x)]\\
&\qquad\quad\times[g_{E_2,\kappa_2}(r_y)f_{E_b,\kappa_b}(r_y)\Xi^*_{j_2,l_2,\mu_2}(\hat\Omega_y)\sigma^i\Xi_{j_b,\bar l_b,\mu_b}(\hat\Omega_y)\\
&\qquad\quad-f_{E_2,\kappa_2}(r_y)g_{E_b,\kappa_b}(r_y)\Xi^*_{j_2,\bar l_2,\mu_2}(\hat\Omega_y)\sigma^i\Xi_{j_b,l_b,\mu_b}(\hat\Omega_y)]\}\ .\end{aligned} \tag{11}$$

The main advantage of this result is that the angular variables are completely separated: each term in the sum has the form

$$T\sim R\langle j_1,l_1,\mu_1|\sigma^\alpha|n,m|j_0,l_0,\mu_0\rangle\times\langle j_2,l_2,\mu_2|\sigma^\alpha|n,m|j_b,l_b,\mu_b\rangle\ , \tag{12a}$$

with

$$\langle j,l,\mu|\sigma^\alpha|n,m|\hat j,\hat l,\hat\mu\rangle=\int d\Omega\,\Xi^*_{j,l,\mu}(\Omega)\sigma^\alpha Y_{n,m}(\Omega)\Xi_{\hat j,\hat l,\hat\mu}(\Omega) \tag{12b}$$

$$R=\int_0^\infty dr_x r_x^2\int_0^\infty dr_y r_y^2 j_n(\rho r_<)[-y_n(\rho r_>)+ij_n(\rho r_>)]\times\phi_1(r_x)\phi_0(r_x)\phi_2(r_y)\phi_b(r_y)\ , \tag{12c}$$

where $\alpha=0,1,2,3$ and each $\phi(r)$ represents a large or small component radial function occurring in (11). The angular integrals (12b) can be worked out analytically and explicit expressions are given in Appendix A. Due to the fact that the distorting potential is not known in closed form, the remaining calculations have to be done numerically.

III. NUMERICAL METHODS

There are two major problems in computing the S-matrix elements from (11), namely, the enormous number of terms contributing to the eleven-fold sum and the evaluation of the individual radial integrals of the form (12c). While highly efficient and accurate methods are available for evaluating the vector coupling coefficients that make up the angular integrals (12b), care has to be taken to include all angular momentum selection rules into the calculation in order to reduce the number of terms. However, the convergence of the various sums has to be studied in detail in order to keep computing time within reasonable limits while incorporating all relevant contributions. This matter will be addressed in Sec. III B.

The main challenge in the computation of the radial integrals (12c) stems from three peculiarities of this task.

(a) The wave-function components $\phi(r)$ are only known analytically in the asymptotic region. It is therefore impossible to tailor the integration algorithm explicitly to the analytical structure of the integrand in the vicinity of the nucleus where one would expect the dominant contributions to the integral.

(b) Due to the large momenta involved, the three scattering wave functions are rapidly oscillating functions.

(c) A highly accurate numerical solution of the integrals is required, since due to the large number of radial matrix elements and the relative signs entering through the vector coupling coefficients, cancellation effects are severe.

In the following discussion, we will restrict ourselves to the case of short-range effective potentials, thus assuming that all distorted waves are generated in the field of a neutral atom. The complications arising from using Coulomb boundary conditions for one or both of the outgoing electrons will be only briefly addressed, a detailed investigation of this matter being reserved for a forthcoming publication.

A. Description of algorithms

The radial integrals (12) may be split up in the form

$$\mathrm{Re}R=\int_0^\infty dr_x r_x^2\phi_1(r_x)\phi_0(r_x)V(r_x)\ , \tag{13a}$$

$$\mathrm{Im}R=C\int_0^\infty dr_x r_x^2\phi_1(r_x)\phi_0(r_x)j_n(\rho r_x)\ , \tag{13b}$$

$$V(r_x)=-y_n(\rho r_x)\int_0^{r_x} dr_y r_y^2 j_n(\rho r_y)\phi_2(r_y)\phi_b(r_y) -j_n(\rho r_x)\int_{r_x}^\infty dr_y r_y^2 y_n(\rho r_y)\phi_2(r_y)\phi_b(r_y)\ , \tag{13c}$$

$$C=\int_0^\infty dr_y r_y^2 j_n(\rho r_y)\phi_2(r_y)\phi_b(r_y)\ . \tag{13d}$$

In order to evaluate these expressions, we solve the radial Dirac equations (7) for the functions ϕ on an equidistant grid using the program package developed by Salvat and Mayol [35], which is based on a power-series expansion [36]. At a maximum radius $R_{\max}$ determined by this code subject to accuracy requirements, the wave functions are matched to radial solutions of the free Dirac equation,

$$g_{E,\kappa}^{\mathrm{asymp}}(r)=\left[\frac{E+c^2}{2E}\right]^{1/2}[\cos(\delta_\kappa)j_l(kr)-\sin(\delta_\kappa)y_l(kr)]\ , \tag{14a}$$

$$f_{E,\kappa}^{\mathrm{asymp}}(r)=\mathrm{sgn}(\kappa)\left[\frac{E+c^2}{2E}\right]^{1/2}\frac{kc}{E+c^2}[\cos(\delta_\kappa)j_{\bar{l}}(kr)-\sin(\delta_\kappa)y_{\bar{l}}(kr)]\ . \tag{14b}$$

The scattering phase shift δ_κ is determined by solving (14a) for δ_κ at the matching point.

The integrands of the "inner" integrals (13c) and (13d) are heavily damped by the exponentially decreasing bound-state wave function, in particular for the large nuclear charges we are interested in. For each target system, it is therefore possible to determine a value of r_x much smaller than $R_{\max}$ at which these integrals practically take their asymptotic values. Between the origin and this point, the integrals (13c) and (13d) are evaluating using fourth-order Newton-Cotes rules on a sufficiently dense grid. The constant C is obtained using the same procedure. We have verified that this method is accurate to at least six significant figures by comparing the results with closed analytical expressions (see Appendix B) and by alternatively calculating C using a high-order Gauss-Legendre rule.

The "outer" integrals (13a) and (13b) are treated in two steps. For the interval $(0,R_{\max})$, a Romberg integration scheme is used. A large number of points (of order 10^4) is required to resolve the rapid oscillations of the integrand. Because of computing time and storage limitations, it is not practicable to refine the grid until a prescribed accuracy is obtained. Rather, we monitor the error estimate returned by the Romberg scheme in order to be able to treat particularly troublesome integrals separately. (It should be noted that the use of higher-order rules like Gaussian formulas is inadequate for the problem at hand because the integrands cannot be appropriately represented by finite order polynomials.)

In the asymptotic region $[R_{\max},\infty)$, according to (13a), (13b), (14a), and (14b), the analytical form of the integrand is known, the integral is a sum of terms of the form

$$\int_{R_{\max}}^{\infty} dr_x r_x^2 b_n(\rho r_x) b_{l_1}(k_1 r_x) b_{l_0}(k_0 r_x) , \tag{15}$$

where the $b_i(z)$ are spherical Bessel functions of the first or second kind. A powerful numerical algorithm for these integrals has been developed in [37]. The basic idea of this approach is to represent the Bessel functions by spherical Hankel functions. This allows the integrand to be split up into contributions that decrease exponentially in the upper or lower half of the complex plane. By appropriate rotations of the integration contour, the individual oscillating terms can thus be converted into smoothly decreasing ones. We have refined this approach by combining it with a Gauss-Laguerre rule. This allows the integrals to be done to high accuracy using only a few points. In our implementation, the results obtained with 15- and 25-point rules differ only in the ninth digit.

To test the combined algorithm, we have extensively studied the integral

$$\int_0^{\infty} dx\, x^2 j_n(\rho x) j_l(kx) j_m(\tilde{k}x) , \tag{16}$$

for which an analytical solution has been found (see [38] and references therein; note also the discussion in Appendix B). We have found that a minimum accuracy of five significant figures can be obtained. Note also that (13b) reduces to (16) if all scattering waves are taken to be plane waves. This provides another severe test of the method since the two parts of the integral have to cancel each other to provide the vanishing imaginary part of the plane-wave S-matrix elements. Indeed, we observe cancellation of at least the leading six figures in all these integrals.

Despite the convincing results obtained in all our test cases, it turns out that there remains the possibility of a systematic error of a few percent in the computation of some of the integrals (13a). This is due to the fact that by construction both the integral (13c) and the integrand of (13a) vary on the scale defined by the zero component ρ of momentum transfer, which leads to very important cancellations that are strongly increased if multiplied by low-order partial waves with relative phase-shift zero. In consequence, there is a certain tendency toward overestimating the leading matrix elements of the multipole sum. Indeed, it will be seen in the following section that our tests within the plane-wave approximation—which represents a worst-case scenario with regard to this problem—are somewhat biased by the effect just described.

While the integration scheme used for the inner part of the integrals does not depend on the analytic structure of the integrand, the algorithm used for the asymptotic part of the outer integrals explicitly uses the Bessel function form of the asymptotic solutions (14). Therefore, the corresponding part of the numerical procedures has to be modified if Coulomb boundary conditions are included. This problem can be approached using a similar contour integration procedure, details of which will be described elsewhere.

B. Convergence studies

In the following, we present a set of calculations using plane waves for all scattering waves. For this problem an analytical solution is possible (see Appendix B). This allows us to assess the quality of our numerical results for complete triple differential cross sections as a function of the number of terms retained in the multipole and angular momentum sums.

We will discuss two example systems: a very asymmetric kinematical situation (ionization of the gold K shell, $E_0=500$ keV, $E_1=319$ keV, $E_2=100$ keV, the fast electron being observed at $-15°$) and a symmetric problem (same target, but at $E_0=300$ keV, $E_1=E_2=109.65$ keV).

The restrictions imposed on the set of partial waves and multipoles considered can be expressed by fixing two quantum numbers. The remaining quantities are then limited by triangle inequalities. In the following, we will therefore discuss our results in the plane-wave approximation as functions of the number of partial waves in the incoming channel (defined by the total angular momentum j_0) and of the number of terms in the expansion of the propagator (the multipolarity n).

We have based our study on a standard set of matrix elements defined by $n \leq 7$ and $j_0 \leq 25$. For asymmetric geometries, an estimate of the number of multipoles based on the Bethe approximation (see Appendix B) suggest that terms beyond $n=7$ are likely to be negligible. The maximum value of j_0 is then dictated by hardware restrictions.

In Figs. 2 and 3 we show the triple differential cross sections for different maximum multipolarities. The convergence of the series is obvious. However, there is a tendency to overestimate the exact result that is most clearly visible in the tip region and right slope of the asymmetric binary peak. This feature is a manifestation of the problem associated with the evaluation of the radial integrals that was discussed at the end of the preceding section.

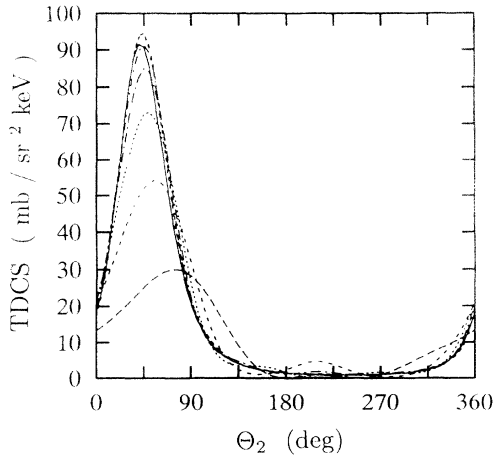

FIG. 2. TDCS for ionization of Au as a function of Θ_2 in the plane-wave approximation. $E_0=500$ keV, $E_2=100$ keV, $\Theta_1=-15°$. Full curve, exact result; broken curves, results for different maximum multipolarities, $n \leq 1$ (long dashes), $n \leq 2$ (short dashes), $n \leq 3$ (dots), $n \leq 4$ (long dash-dotted line), $n \leq 5$ (short dash-dotted line), $n \leq 6$ (double short dashes), $n \leq 7$ (triple short dashes). (The last two lines are almost indistinguishable in this plot.)

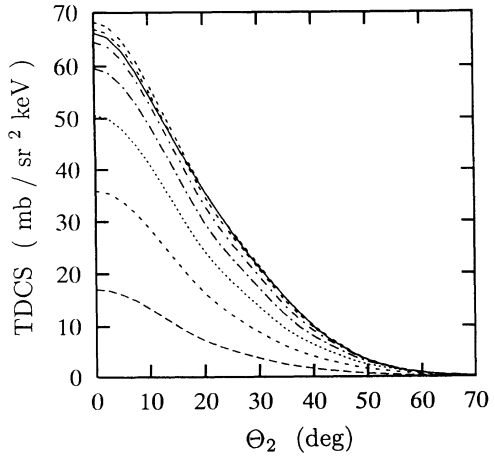

FIG. 3. TDCS for ionization of Au as a function of Θ_2 in the plane-wave approximation. $E_0=300$ keV, $E_2=E_1=109.65$ keV. Symbols are as in Fig. 2.

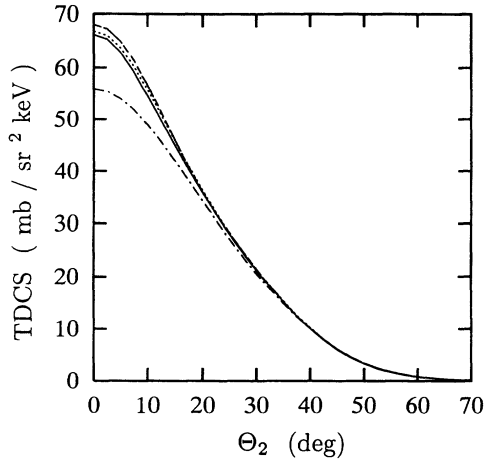

FIG. 5. Same as Fig. 3, but for maximum multipolarity $n=7$ and different maximum angular momentum j_0 in the incident channel. Symbols are as in Fig. 4.

The data for asymmetric geometry clearly show that the error described above is to be attributed to an overestimation of the maxima of the low multipolarity terms. However, we emphasize again that the plane-wave calculations are particularly sensitive to this type of deviation because of the vanishing relative phases within the individual matrix elements. Figures 4 and 5 indicate that the deviation described cannot be attributed to an incomplete summation of angular momenta. Note that the differences between the calculations with $j_0 \leq 20$ and $j_0 \leq 25$ are almost invisible in the plots.

These results clearly indicate that this standard set of angular momentum and multipole contributions is adequate for the theoretical description of the kinematic configurations of interest. (Of course, proper convergence of the multiple sum is verified in each individual calculation.) Furthermore, from the data presented, a very conservative error estimate of our calculation may be extracted. Our calculations are at no point more than 10% off the exact result. However, this includes the systematic error discussed above that accounts for most of the discrepancies (as is evidenced by a detailed analysis of selected individual matrix elements). For a realistic calculation, where the nontrivial scattering phases induce additional error cancellations that are absent in the plane-wave case, we can therefore use our standard set of parameters to an expected maximum error of a few percent.

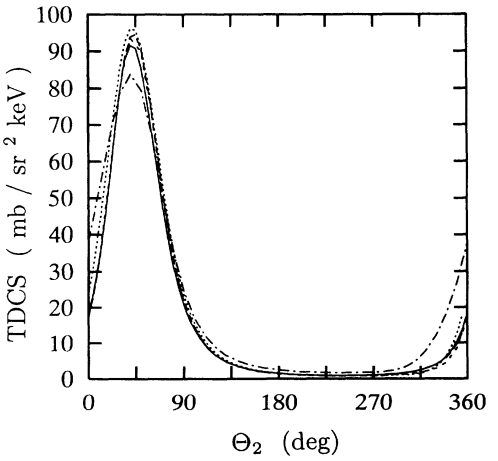

FIG. 4. Same as Fig. 2, but for maximum multipolarity $N=7$ and different maximum angular momentum j_0 in the incident channel. Full curve: exact result; long dashed curve: $j_0 \leq 25$; short dashed curve: $j_0 \leq 20$; dotted curve: $j_0 \leq 15$; dash-dotted curve: $j_0 \leq 10$.

As a complementary check of our program, we have verified that the nonrelativistic DWBA results for electron-impact ionization of the neon K shell published in [13] are reproduced. While the plane-wave case is extremely sensitive to errors in the integration algorithms and the handling of all the relativistic extensions of the standard theory, this test allowed us to make sure that the influence of the distorted potential on the wave functions is properly incorporated.

IV. APPLICATIONS

Absolute measurements (with a systematic error of 15%) of TDCS for relativistic $(e,2e)$ processes in asymmetric geometry have been carried out by Nakel and collaborators for gold and silver targets. In Fig. 6, we compare their results for a gold target ($E_0=500$ keV, $E_1=100$ keV, $\Theta_1=-15°$) with theoretical results by Das and Konar [10], who use a semirelativistic Sommerfeld-Maue Coulomb wave function to represent the slow outgoing electron and the Ochkur approximation for the exchange term, and with the first Born results of Walters *et al.* [7], where a Darwin-Coulomb wave is used for this electron. Both theories employ plane waves to describe the incoming and fast outgoing electron, and they both overestimate the experiment by about a factor of 4. (It is not clear why the calculation of Das and Konar mispredicts the location of the maximum). As may be

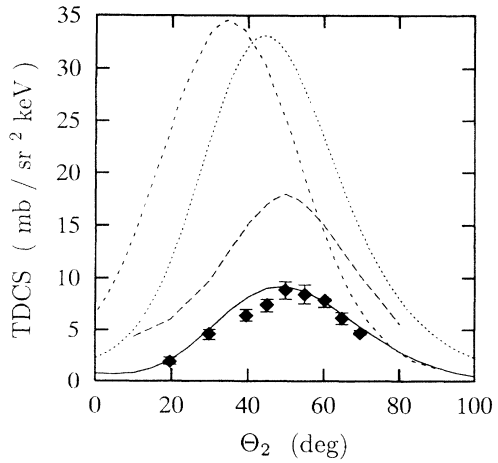

FIG. 6. TDCS for $(e,2e)$ on gold, $E_0=500$ keV, $E_2=100$ keV, $\Theta_1=-15°$. Full squares: experimental results [6]; short dashed curve: results from Das and Konar [10]; dotted curve: first Born approximation (Walters *et al.* [7]); long dashed curve: Coulomb-Born approximation (Jakubaβa-Amundsen [11]); full curve: this work.

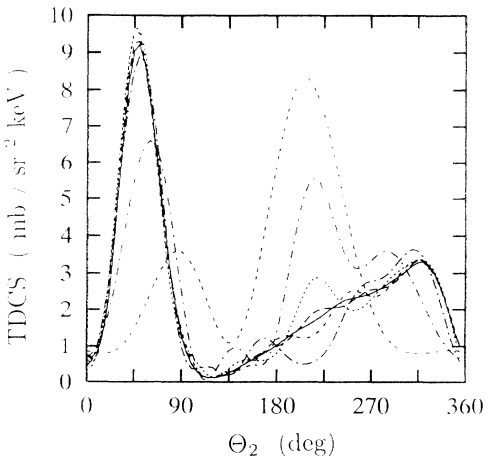

FIG. 7. Convergence of multipole series for the calculation of Fig. 6. Full curve: final result ($n \leq 7$); broken curves: results for different maximum multipolarities, $n \leq 6$ (long dashes), $n \leq 5$ (short dashes), $n \leq 4$ (dots), $n \leq 3$ (long dash-dotted line), $n \leq 2$ (short dash-dotted line), $n \leq 1$ (double dashes).

seen from Figs. 2 and 4, using plane waves in all channels would lead to an order-of-magnitude deviation from the experimental results. Furthermore, Fig. 6 shows the result of a Coulomb-Born calculation by Jakubaβa-Amundsen [11]. The results of this theory, which may be understood as an approximation to the full DWBA, as was indicated in the Introduction, is much closer to the experimental data but still overpredicts them by a factor of 2. Finally, we show a calculation in the relativistic DWBA. A self-consistent relativistic Kohn-Sham local-density approximation (LDA) potential [39] (which is essentially equivalent to a Dirac-Fock-Slater potential) of a neutral gold atom has been used in all channels. The bound state was described by a relativistic hydrogenic $1s_{1/2}$ wave function. The effects of Slater screening and of orthogonalizing the outgoing distorted waves to the bound state were found to be negligible. The standard set of angular momenta and multipoles discussed in the preceding section was used. Figure 7 demonstrates that the convergence of the multiple series is almost perfect over the whole range of angles. From the various theoretical results, it is obvious that for this heavy target the process in question may be understood as a first-order process in the electron-electron interaction that occurs in the strong Coulomb field of the nucleus and the spectator electrons.

In Figs. 8 and 9, we show the same theories for the two experiments that have been carried out with silver targets ($E_0=500$ keV, $E_2=100$ keV, $\Theta_1=-7°$, and $\Theta_1=-15°$). Unfortunately, no Coulomb-Born calculation has been published for the latter system. As one would expect, the agreement of the approximate first-order theories with the experiments in the region of the "binary" peak is somewhat improved because here the atomic field is substantially weaker. However, the experiment clearly establishes the existence of a second maximum at about $-50°$. Previous theories have not even been able to describe the order of magnitude of this structure relative to the "binary" peak. Again, the relativistic DWBA is quite successful in this respect. The discrepancy between theory and experiment at $\Theta_2=-50°$ is presently being reconsidered both theoretically and experimentally. As is most clearly visible in Fig. 9, for this lighter target the relativistic DWBA also has a certain tendency to overpredict the binary maximum.

Up to now, the additional peak in the recoil regime (which appears in the forward direction due to relativistic kinematics) has only been observed in the above-mentioned experiment with a silver target. The fact that only the DWBA is able to predict it indicates that this structure should be understood as an effect of the electron-atom interaction and hence should depend strongly on the nuclear charge. In Fig. 10, we show

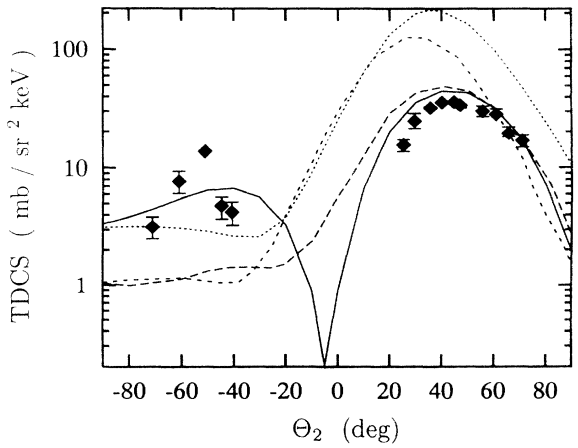

FIG. 8. TDCS for $(e,2e)$ on silver, $E_0=500$ keV, $E_2=100$ keV, $\Theta_1=-7°$. Symbols as in Fig. 6.

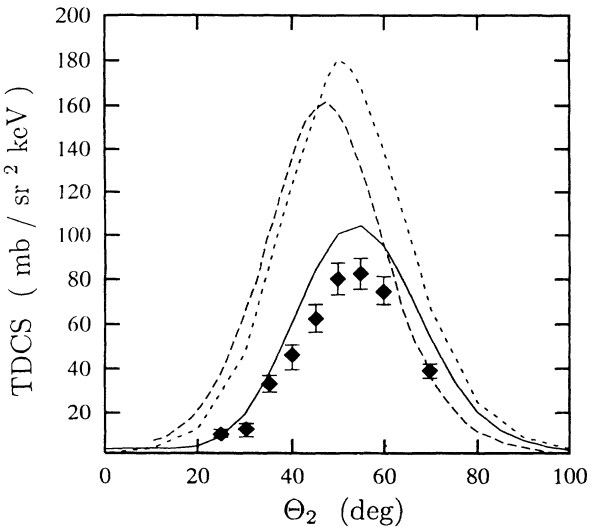

FIG. 9. TDCS for $(e,2e)$ on silver, $E_0=500$ keV, $E_2=100$ keV, $\Theta_1=-15°$. Full squares experimental results [6]; long dashed curve, results from Das and Konar [10]; short dashed curve, first Born approximation (Walters *et al.*[7]); full curve, this work.

TDCS for the kinematical configuration of Fig. 8 ($E_0=500$ keV, $E_2=100$ keV, $\Theta_1=-7°$) and for different atoms, where in each case the maximum of the binary peak has been normalized to unity. Our calculations indicate a drastic buildup of the relative magnitude of the secondary maximum. It is gratifying to note that this increase leads to secondary peak cross sections of the order of a few millibarn for all targets. Therefore, it should be possible to detect this structure with the present experimental setup of the Tübingen group and thus test the predicted increase.

Another quite surprising fact is that the shape of the

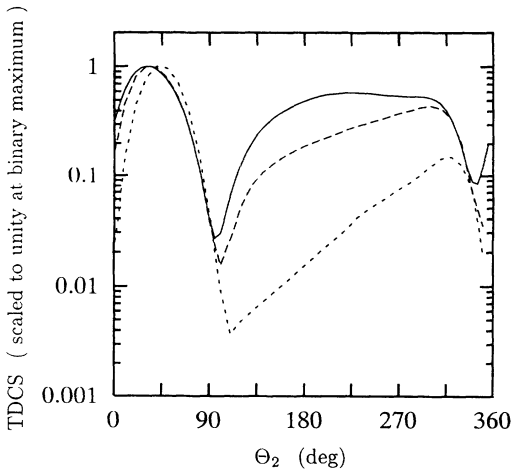

FIG. 10. Relativistic DWBA calculations for TDCS at $E_0=500$ keV, $E_2=100$ keV, $\Theta_1=-7°$ with different targets. Cross sections normalized to unity at the maximum of the binary peak. Full curve, uranium target; long dashed curve, gold target; short dashed curve, silver target.

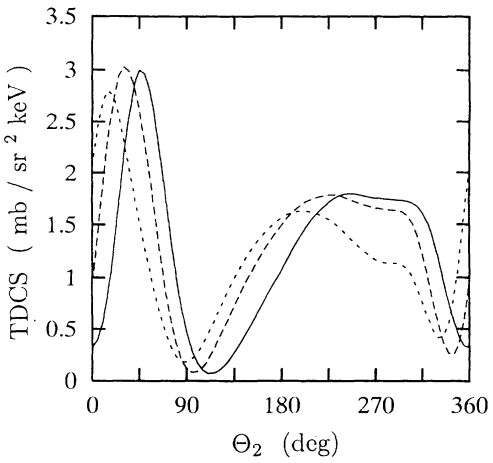

FIG. 11. Relativistic DWBA calculations for TDCS at $E_0=500$ keV, $E_2=100$ keV, uranium target. Full curve, $\Theta_1=-15°$; long dashed curve, $\Theta_1=-7°$; short dashed curve, $\Theta_1=-3.5°$.

secondary peak changes significantly. While for gold and silver it takes the form of a well-defined maximum with a slowly increasing left slope, a plateaulike structure develops in the case of uranium (see Fig. 11). Note also that the magnitudes of both binary and secondary maxima are almost independent of the detection angle of the fast electron. For very small angles, the TDCS decreases, an effect most prominent in the region of the beam axis. The plateau structure reduces to a saddle in the secondary maximum, which then takes its maximum value in the backward direction. The question whether or not these unusual features of the TDCS exist makes experiments with uranium targets particularly desirable.

V. SUMMARY AND OUTLOOK

In this contribution, we derive the relativistic distorted-wave Born approximation for $(e,2e)$ processes, which is equivalent to a consistent first-order QED calculation in the Furry picture. The numerical methods required for the practical application of this theory are presented and the convergence of the angular momentum and multipole expansions is discussed in some detail. It is demonstrated that the triple differential cross sections of interest may be calculated to a numerical error of at most a few percent.

The comparison of our numerical results with data from absolute measurements in asymmetric geometry shows that these relativistic $(e,2e)$ processes may adequately be described in terms of a binary collision of the electrons, provided that the influence of the electric field of the nucleus and the other atomic electrons is properly incorporated. The secondary maximum in the forward direction, whose existence is established experimentally but has failed to be described by all previous theories, then emerges naturally. We predict an important increase of the relative magnitude and a broadening of this structure as a function of the nuclear charge. Both

effects should be observable with present experimental techniques.

A set of calculations in symmetric geometry is now near completion. These results will be presented in a forthcoming paper [42]. We are presently involved in extending our code to include Coulomb boundary conditions and a spin-polarized incident channel. It is to be expected that by proceeding along these lines while maintaining a close collaboration with the experimentalists, the understanding of the physics of relativistic $(e,2e)$ processes will be further improved.

ACKNOWLEDGMENTS

We are most grateful to Professor Werner Nakel and his collaborators for many enlightening discussions. Support by the European Science Foundation (REHE program), the Deutsche Forschungsgemeinschaft, the DAAD and British Council (ARC), the EC (Human Capital and Mobility Program), SERC, and NATO (CRG 920101) is gratefully acknowledged. The numerical calculations have been performed on the RISC workstations of the Gesellschaft für Schwerionenforschung, Darmstadt, and the Institut für Theoretische Physik, Frankfurt.

APPENDIX A: ANGULAR INTEGRALS

The angular integrations in

$$\langle j,l,\mu|\sigma^{\alpha}|N,M|\hat{j},\hat{l},\hat{\mu}\rangle = \int d\Omega\, \Xi^{*}_{j,l,\mu}(\Omega)\sigma^{\alpha}Y_{N,M}(\Omega)\Xi_{\hat{j},\hat{l},\hat{\mu}}(\Omega)\ ,$$

may be performed by inserting the explicit form of the spinorial harmonics and using

$$\int d\Omega\, Y^{*}_{l,\mu-m}(\Omega)Y_{N,M}(\Omega)Y_{\hat{l},\hat{\mu}-\hat{m}}(\Omega)=\delta_{M+\hat{\mu}-\hat{m},\mu-m}\left[\frac{(2N+1)(2\hat{l}+1)}{4\pi(2l+1)}\right]^{1/2} \times C(N,\hat{l},l,0,0,0)C(N,\hat{l},l,M,\hat{\mu}-\hat{m},\mu-m) \tag{A1}$$

to find

$$\langle j,l,\mu|\sigma^{\alpha}|N,M|\hat{j},\hat{l},\hat{\mu}\rangle = \left[\frac{(2N+1)(2\hat{l}+1)}{4\pi(2l+1)}\right]^{1/2} C(N,\hat{l},l,0,0,0) \times \sum_{m=-1/2}^{1/2}\chi^{T}(m)\sigma^{\alpha}\chi(M+m+\hat{\mu}-\mu)C(N,\hat{l},l,M,\mu-m-M,\mu-m) \times C(\hat{l},\tfrac{1}{2},\hat{j},\mu-m-M,\hat{\mu}-\mu+m+M,\hat{\mu})C(l,\tfrac{1}{2},j,\mu-m,m,\mu)\ . \tag{A2}$$

In the remaining sum, the bilinear forms $\chi^{T}\sigma^{\alpha}\chi$ may be written as

$$\chi^{T}(m)\sigma^{0}\chi(M+m+\hat{\mu}-\mu)=\delta_{m,M+\hat{\mu}+m-\mu}\ , \tag{A3a}$$

$$\chi^{T}(m)\sigma^{1}\chi(M+m+\hat{\mu}-\mu)=\delta_{m-M-\hat{\mu}-m+\mu}\ , \tag{A3b}$$

$$\chi^{T}(m)\sigma^{2}\chi(M+m+\hat{\mu}-\mu)=-2im\,\delta_{m,-M-\hat{\mu}-m+\mu}\ , \tag{A3c}$$

$$\chi^{T}(m)\sigma^{3}\chi(M+m+\hat{\mu}-\mu)=2m\,\delta_{m,M+M+\hat{\mu}+m-\mu}\ . \tag{A3d}$$

This can be used to collapse the summation over M in the $\alpha=0$ and $\alpha=3$ terms, thus simplifying the calculation considerably. For the other terms, it is more useful to the compute the m sum instead. The final results for the angular integrals read [with $W(\ldots)$ a Racah symbol]

$$\langle j,l,\mu|\sigma^{0}|N,M|\hat{j},\hat{l},\hat{\mu}\rangle=\delta_{M,\mu-\hat{\mu}}(-1)^{l+1/2-\hat{j}+\hat{\mu}-\mu}\left[\frac{(2N+1)(2\hat{l}+1)(2j+1)}{4\pi}\right]^{1/2} \times C(N,\hat{l},l,0,0,0)W(j,l,\hat{j},\hat{l};\tfrac{1}{2},N)C(j,N,\hat{j},\mu,\hat{\mu}-\mu,\hat{\mu})\ , \tag{A4a}$$

$$\langle j,l,\mu|\sigma^{1}|N,M|\hat{j},\hat{l},\hat{\mu}\rangle = \left[\frac{(2N+1)(2\hat{l}+1)}{4\pi(2l+1)}\right]^{1/2} C(N,\hat{l},l,0,0,0)C\left[N,\hat{l},l,M,\frac{\mu+\hat{\mu}-M}{2},\frac{\mu+\hat{\mu}+M}{2}\right] \times C\left[l,\tfrac{1}{2},j,\frac{\mu+\hat{\mu}+M}{2},\frac{\mu-\hat{\mu}-M}{2},\mu\right]C\left[\hat{l},\tfrac{1}{2},\hat{j},\frac{\mu+\hat{\mu}-M}{2},\frac{\mu-\hat{\mu}+M}{2},\hat{\mu}\right]\ , \tag{A4b}$$

$$\langle j,l,\mu|\sigma^{2}|N,M|\hat{j},\hat{l},\hat{\mu}\rangle = -2i\frac{\mu-\hat{\mu}-M}{2}\left[\frac{(2N+1)(2\hat{l}+1)}{4\pi(2l+1)}\right]^{1/2} C(N,\hat{l},l,0,0,0)C\left[N,\hat{l},l,M,\frac{\mu+\hat{\mu}-M}{2},\frac{\mu+\hat{\mu}+M}{2}\right] \times C\left[l,\tfrac{1}{2},j,\frac{\mu+\hat{\mu}+M}{2},\frac{\mu-\hat{\mu}-M}{2},\mu\right]C\left[\hat{l},\tfrac{1}{2},\hat{j},\frac{\mu+\hat{\mu}-M}{2},\frac{\mu-\hat{\mu}+M}{2},\hat{\mu}\right]\ , \tag{A4c}$$

$$\langle j,l,\mu|\sigma^3|N,M|\hat{j},\hat{l},\hat{\mu}\rangle=\delta_{M,\mu-\hat{\mu}}\left[\frac{(2N+1)(2\hat{l}+1)}{4\pi(2l+1)}\right]^{1/2}C(N,\hat{l},l,0,0,0)$$
$$\times\sum_{m=-1/2}^{1/2}2mC(N,\hat{l},l,\mu-\hat{\mu},\hat{\mu}-m,\mu-m)$$
$$\times C(l,\tfrac{1}{2},j,\mu-m,m,\mu)C(\hat{l},\tfrac{1}{2},\hat{j},\mu-\hat{\mu},\hat{\mu}-m,\mu-m)\ . \tag{A4d}$$

APPENDIX B: ANALYTICAL BENCHMARK RESULTS

In order to be able to assess the proper implementation and quality of the algorithms, analytical test cases are indispensable in any numerical work. Since in the literature there are only very few closed results available for relativistic $(e,2e)$ processes, we summarize in this Appendix some of the results we have derived in order to test our code.

The main approximation used in all our analytical calculations is that of replacing the distorted waves with plane-wave states. This is consistent with our present restriction to short-range potentials. In this case, the triple differential cross section can be worked out in closed form. It should be noted that in order to be able to check the individual spin contributions separately, the calculation must not be simplified by using trace identities. Therefore, the result is too long to be reproduced here. For a discussion of this approximation see [44].

In the plane-wave approximation, Eq. (12c) reduces to

$$R=A\int_0^\infty dr_x r_x^2\int_0^\infty dr_y r_y^2 j_n(\rho r_>)[-y_n(\rho r_<)+ij_n(\rho r_<)]j_{l_1}(k_1 r_x)j_{l_0}(k_0 r_x)j_{l_2}(k_2 r_y)\phi_b(r_y)\ , \tag{B1}$$

where l_i may correspond to κ or $-\kappa$ and A is a normalization factor, depending on the choice of large and small components involved. While it is possible to calculate the leading matrix elements (B1) in closed form by inserting the explicit representation of the spherical Bessel functions in terms of trigonometric functions and approximating the bound-state wave function by its nonrelativistic limit, the resulting expressions are only finite due to subtle cancellations between a number of terms of a much different structure. This makes them quite susceptible to numerical errors themselves, so that they are not useful for testing other programs.

In order to construct closed expressions for the individual radial matrix elements (12c), we further apply a relativistic analog of the Bethe approximation discussed in [40]. It corresponds to the assumption that r_x is always the larger of the two radial coordinates. Owing to the fact that $\phi_b(r_y)$ is a rapidly decreasing function and that $j_l(x)\sim x^l$ for small x, this approximation is well justified for the contributions from high multipoles and angular momenta. Of course, the low-order terms are misrepresented so that the results for triple differential cross sections cannot be expected to be consistent with experimental data. In particular, this restriction applies to symmetric geometries where the momentum transfer to the nucleus is large.

Under the assumption stated above, (B1) factorizes:

$$R=ABC\ ,$$
$$B=\int_0^\infty dr_x r_x^2[-y_n(\rho r_x)+ij_n(\rho r_x)]\times j_{l_1}(k_1 r_x)j_{l_0}(k_0 r_x)\ , \tag{B2a}$$
$$C=\int_0^\infty dr_y r_y^2 j_n(\rho r_y)j_{l_2}(k_2 r_y)\phi_b(r_y)\ . \tag{B2b}$$

Note that C is identical to (13d) written in the plane-wave approximation. To check the algorithm used for the inner integrals for all combinations of large and small components, we have evaluated (B2b) for $(n=0,\ l_2=0)$, $(n=1,\ l_2=0)$, and $(n=0,\ l_2=1)$ using a relativistic hydrogenic $1s$ state:

$$C_{nl}:=\int_0^\infty dr\, r^2 j_n(\rho r)j_l(kr)r^{\gamma-1}e^{-Zr} \tag{B3a}$$
$$C_{00}=\frac{1}{2k\rho}[Fc(\rho-k,\gamma)-Fc(\rho+k,\gamma)]\ ,$$
$$C_{10}=\frac{1}{2k\rho^2}[Fc(-\rho+k,\gamma-1)-Fc(\rho+k,\gamma-1)]+\frac{1}{2k\rho}[Fs(\rho-k,\gamma)-Fs(\rho+k,\gamma)]\ , \tag{B3b}$$
$$C_{01}=\frac{1}{2k\rho^2}[Fc(\rho-k,\gamma-1)-Fc(\rho+k,\gamma-1)]+\frac{1}{2k\rho}[Fs(-\rho+k,\gamma)-Fs(\rho+k,\gamma)]\ , \tag{B3c}$$
$$Fc(a,b):=\frac{\Gamma(b)}{(a^2+Z^2)^{b/2}}\cos\left[b\arctan\left[\frac{a}{Z}\right]\right]\ , \tag{B3d}$$
$$Fs(a,b):=\frac{\Gamma(b)}{(a^2+Z^2)^{b/2}}\sin\left[b\arctan\left[\frac{a}{Z}\right]\right]\ , \tag{B3e}$$

where $\gamma=[1-(Z^2/c^2)]^{1/2}$, and we have omitted all normalizing factors in the displayed equations.

The integrals with three Bessel functions of the first kind arising from (B2a) has been solved in a form that is readily evaluated numerically ([38]: see also the very recent study [41]). As these integrals occur quite frequently (actually, whenever a plane-wave approximation is evaluated with a multipole expanded photon or meson propagator), their analytical evaluation continues to be of considerable importance.

Finally, the Bethe approximation allows for an estimate of the number of multipoles required in our calculations in asymmetric geometry. To this end, one has to compute (B2b) as a function of n. This is feasible if the bound state is treated in the nonrelativistic approximation. Again, the various combinations of l_2 and n have to be considered. We give here only the result for $l_2=n$ corresponding to combining the large components of both wave functions. The other combinations of large and small components lead to similar expressions. For the $1s\frac{1}{2}$ state we find ($n>0$) [43]

$$M_{1s1/2}(n):=\int_0^\infty dr\, r^2 e^{-Zr} j_n(\rho r) j_n(kr) = -\frac{2Z}{(2\rho k)^2}(u^2-1)^{-1/2} Q_n^1(u)\ , \tag{B4a}$$

where $Q_n^i(u)$ is an associated Legendre function of the second kind and

$$u=\frac{Z^2+\rho^2+k^2}{2\rho k}\ . \tag{B4b}$$

The calculation can be repeated for the $2P_{3/2}$ state. The corresponding result reads ($n>1$)

$$M_{2p_{3/2}}(n):=\int_0^\infty dr\, r^3 e^{-Z/2r} j_n(\rho r) j_{n\pm1}(kr) = -\frac{8Z}{(8\rho k)^3}(u^2-1)^{-1}[\rho Q_n^2(u)-kQ_{n-1}^2(u)]\ , \tag{B5}$$

where Z has to be replaced by $Z/2$ in (B4b). Figure 12 shows the absolute values of these functions (for $Z=79$, $E_0=500$ keV, $E_2=100$ keV), both normalized to unity at $n=2$. It is evident that although both types of inner integrals go down exponentially for large enough n, the multipole series will converge much slower for L-shell states.

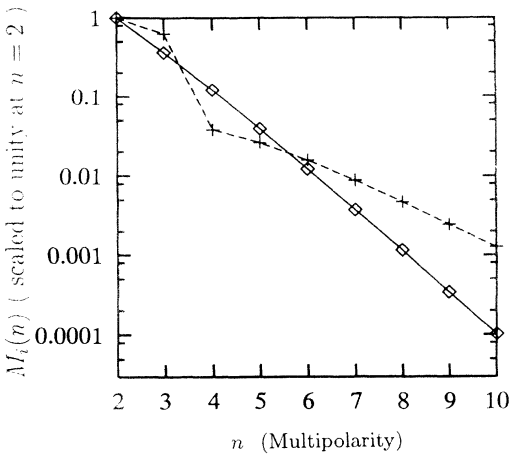

FIG. 12. Absolute values of $M_{1s1/2}$ (squares) and $M_{2p3/2}$ (crosses) as defined by Eqs. (B4) and (B5), normalized to unity at $n=2$.

[1] H. Ehrhardt, M. Schulz, T. Tekaat, and K. Willmann, Phys. Rev. Lett. **22**, 69 (1969).
[2] U. Amaldi, A. Egidi, R. Marconero, and G. Pizella, Rev. Sci. Instrum. **40**, 1001 (1969).
[3] *(e,2e) and Related Processes,* edited by C. T. Whelan, H. R. J. Walters, A. Lahmam-Bennani, and H. Erhardt (Kluwer, Dordrecht, 1993).
[4] E. Schüle and W. Nakel, J. Phys. B **15**, L639 (1982).
[5] H. Ruoff and W. Nakel, J. Phys. B **20**, 2299 (1987).
[6] J. Bonfert, H. Graf, and W. Nakel, J. Phys. B **24**, 1423 (1991).
[7] H. R. J. Walters, H. Ast, C. T. Whelan, R. M. Dreizler, H. Graf, C. D. Schröter, J. Bonfert, and W. Nakel, Z. Phys. D **23**, 353 (1992).
[8] C. D. Schröter, H. Th. Prinz, N. Keuler, and W. Nakel, in *(e,2e) and Related Processes* (Ref. [3]), p. 403.
[9] F. Bell, J. Phys. B **22**, 287 (1989).
[10] J. N. Das and A. N. Konar, J. Phys. B **7**, 2417 (1974).
[11] D. H. Jakubaβa-Amundsen, Z. Phys. D **11**, 305 (1989).
[12] D. H. Jakubaβa-Amundsen, J. Phys. B **25**, 1297 (1992).
[13] X. Zhang, C. T. Whelan, H. R. J. Walters, R. J. Allan, P. Bickert, W. Hink, and W. Schönberger, J. Phys. B **25**, 4325 (1992).
[14] C. T. Whelan, R. J. Allan, H. R. J. Walters, and X. Zhang, in *(e,2e) and Related Processes* (Ref. [3]), p. 1.
[15] J. Botero and J. H. Macek, Phys. Rev. A **45**, 154 (1992).
[16] S. R. Lin, Phys. Rev. A **133**, 965 (1964).
[17] H. K. Tseng and R. H. Pratt, Phys. Rev. A **3**, 100 (1971).
[18] M. S. Pindzola and M. J. Buie, Phys. Rev. A **37**, 3232 (1988).
[19] M. S. Pindzola, D. L. Moore, and D. C. Griffin, Phys. Rev. A **40**, 4941 (1989).
[20] D. L. Moores and M. S. Pindzola, Phys. Rev. A **41**, 3603 (1990).
[21] D. L. Moores and M. S. Pindzola, Phys. Rev. A **42**, 5384 (1990).
[22] M. S. Pindzola, Phys. Rev. A **45**, 4530 (1992).
[23] M. N. Butler, M. C. Chu, S. Koonin, and J. Piekarewicz, Phys. Rev. A **38**, 2274 (1988).
[24] H. Ast, S. Keller, C. T. Whelan, H. R. J. Walters, and R. M. Dreizler, Phys. Rev. A **50**, R1 (1994).
[25] C. Hofmann, J. Reinhardt, W. Greiner, G. Schlüter, and G. Soff, Phys. Rev. C **4**, 2632 (1990).
[26] E. H. Wichmann and N. M. Kroll, Phys. Rev. **101**, 843 (1956).
[27] G. Soff and P. J. Mohr, Phys. Rev. A **38**, 5066 (1988).
[28] P. J. Mohr and G. Soff, Phys. Rev. Lett. **70**, 158 (1993).
[29] A. Scherdin, A. Schäfer, W. Greiner, and G. Soff, Phys. Rev. D **45**, 2982 (1992).
[30] W. H. Furry, Phys. Rev. **81**, 115 (1951).
[31] S. S. Schweber, *An Introduction to Relativistic Quantum Field Theory* (Row, Petersen, New York, 1961), p. 472.
[32] E. R. Edmonds, *Angular Momentum in Quantum Theory* (Princeton University Press, Princeton, NJ, 1957).
[33] M. E. Rose, *Relativistic Electron Theory* (Wiley, New York, 1961).

[34] J. Augustin, B. Müller, and W. Greiner, Z. Phys. D **14**, 317 (1989).
[35] F. Salvat and R. Mayol, Comput. Phys. Commun. **62**, 65 (1991).
[36] W. Bühring, Z. Phys. **187**, 180 (1965).
[37] K. T. R. Davies, M. R. Strayer, and G. D. White, J. Phys. G **14**, 961 (1988).
[38] C. T. Whelan, J. Phys. B **23**, L823 (1993).
[39] R. M. Dreizler and E. K. U. Gross, *Density Functional Theory* (Springer, Berlin, 1990).
[40] C. T. Whelan, J. Phys. B **19**, 2343 (1986).
[41] I. P. Grant and H. M. Quiney, J. Phys. A **26**, 7547 (1993).
[42] C. T. Whelan, H. Ast, S. Keller, H. R. J. Walters, and R. M. Dreizler (unpublished).
[43] B. Piraux and C. T. Whelan, Math. Proc. Cambridge Philos. Soc. **101**, 375 (1987).
[44] S. Keller and C. T. Whelan (unpublished).